Biosensors and Bioelectronics 112 (2018) 72–78

Contents lists available at ScienceDirect

Biosensors and Bioelectronics

journal homepage: www.elsevier.com/locate/bios

Molecularly imprinted polymers-based electrochemical DNA biosensor for the determination of BRCA-1 amplified by SiO_2@Ag

Min You, Shuai Yang, Wanxin Tang, Fan Zhang*, Pingang He

School of Chemistry and Molecular Engineering, East China Normal University, Shanghai 200241, PR China

ARTICLE INFO

Keywords:
Electrochemical DNA biosensor
Molecularly imprinted polymers
Rhodamine B
Homogeneous hybridization
Signal amplification

ABSTRACT

A novel electrochemical DNA (E-DNA) biosensing strategy was designed and used for the detection of breast cancer susceptibility gene (BRCA-1). The biosensor was based on gold nanoparticles-reduced graphene oxide (AuNPs-GO) modified glass carbon electrode (GCE) covered with the layer of molecularly imprinted polymers (MIPs) synthesized with rhodamine B (RhB) as template, methacrylic acid (MAA) as the monomer, and Nafion as additive. The signal amplification tracing tag SiO_2@Ag NPs were prepared by covering AgNPs on the surface of SiO_2 nanoparticles in situ, and then DNA probes were modified on AgNPs by Ag-S bond, forming the composites SiO_2@Ag/DNA. In presence of target DNA (T-DNA), homogeneous hybridization was performed with SiO_2@Ag/DNA and RhB labeled DNA, and the resulting SiO_2@Ag/dsDNA/RhB was specifically recognized by MIPs via the interaction between imprinting cavities and RhB. Under optimal conditions, the proposed biosensor exhibited wide linear range from 10 fM to 100 nM, low detection limit of 2.53 fM (S/N = 3), excellent selectivity, reproducibility, stability, and feasibility in serum analysis. Overall, these findings suggest the promising prospects of the proposed biosensing strategy in clinical diagnostics.

1. Introduction

In the past decades, DNA detection methods have attracted tremendous attention due to their pertinent applications, notably in molecular diagnostics and early diagnosis of different diseases, such as genetic disorders, cancer, viral infection, and chronic diseases (Farjami et al., 2011; Mahshid et al., 2015; Saito et al., 2012). Varieties strategies have recently been employed for the manufacturing of DNA sensing platforms (Du and Dong, 2017; Zhao et al., 2015), including optical (Wang et al., 2013), electrochemical (Ling et al., 2015), mass spectrometric (Tretyakova et al., 2013), chromatographic (Nagai et al., 2016) and microgravimetric analysis (Becker and Cooper, 2011). Among these, electrochemical DNA sensing has attracted increasing attention due to its high sensitivity and selectivity, rapid response, amenability to miniaturization, simple instrumentation, and low cost (Diculescu et al., 2016; Palecek and Bartosik, 2012). However, most of the E-DNA sensing approaches require immobilization of the DNA probes on the electrode surface (Drummond et al., 2003; Xiao et al., 2009), which undoubtedly results in lower recognition efficiency and speed with targets when compared to homogeneous recognition. Therefore, homogeneous electrochemical aptasensing strategies were used to take full advantage of their high recognition efficiencies, configurational freedom of probes, and preservation of DNA under physiological conditions (Zhang et al., 2016, 2013). On the other hand, the electroactive substances in most homogeneous E-DNA detection are freely dispersed in solutions, leading to limited sensitivities.

To enhance response signals in homogeneous E-DNA biosensor, several approaches have been developed to capture the electroactive substances from solution to the electrode surface, including host-guest interaction (Cui et al., 2014), π-π stacking interaction (Wang et al., 2015), thiol self-assembly (Hong et al., 2017), biotin-avidin interaction (Zhang et al., 2005), and molecular imprinting adsorption (Tiwari et al., 2012). Among these techniques, molecular imprinting adsorption offers a promising approach to improve sensitivity and selectivity of homogeneous E-DNA biosensors. This is due to recognition of target molecules by MIPs through the specific size, shape, and functionality of three-dimensional imprinting cavities (Yoshikawa et al., 2016), displaying the outstanding affinity. Moreover, MIPs often exhibit better stability than natural biomolecules (Schirhagl, 2014; Wackerlig et al., 2016), coupled with easy preparation and extensive application in biosensing.

In this study, a novel homogeneous electrochemical DNA biosensing strategy with high sensitivity and selectivity was developed based on the specific recognition of MIPs and the signal amplification using SiO_2@Ag nanoparticles. As illustrated in Scheme 1, the target DNA homogeneously hybridized with SiO_2@Ag modified DNA and RhB

* Corresponding author.
E-mail address: fzhang@chem.ecnu.edu.cn (F. Zhang).

https://doi.org/10.1016/j.bios.2018.04.038
Received 25 December 2017; Received in revised form 14 April 2018; Accepted 17 April 2018
Available online 18 April 2018
0956-5663/ © 2018 Elsevier B.V. All rights reserved.

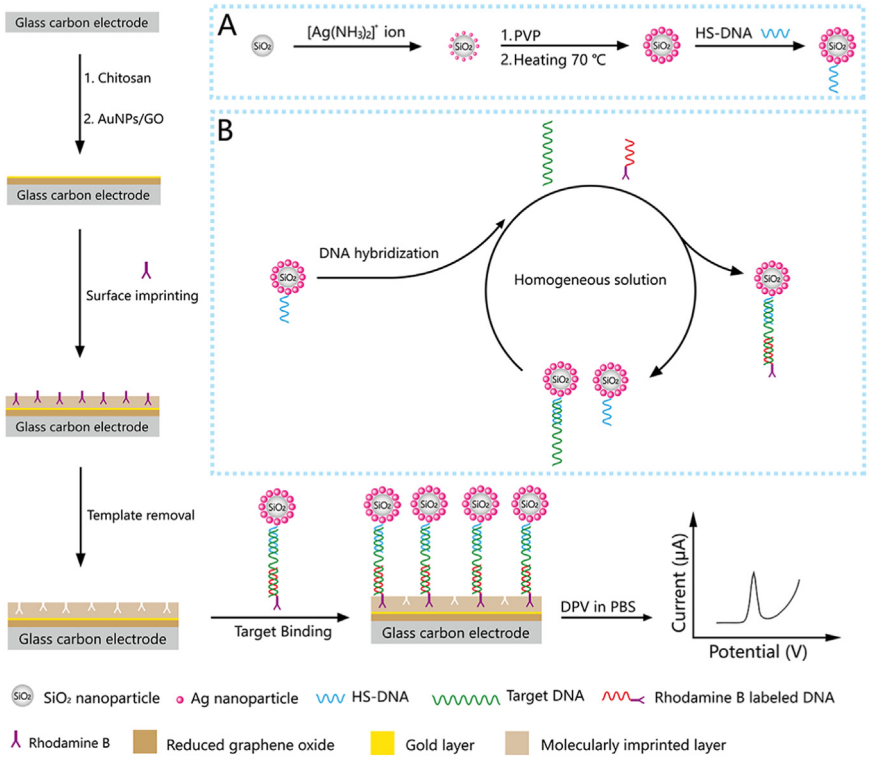

Scheme 1. Schematic illustration of the MIPs-based E-DNA biosensing. Inset of (A) and (B) display the preparation of SiO_2@Ag/DNA and homogeneous DNA hybridization.

labeled DNA, forming the recognizable nanocomposite SiO_2@Ag/dsDNA/RhB. This resulting nanocomposite was transferred from solution to the MIPs modified electrode surface thanks to the recognition of imprinting cavities to RhB. This yielded an amplified electrochemical signal with a detection limit down to 2.53 fM (S/N = 3), coupled with high selectivity and promising applicability in real samples.

2. Experimental sections

2.1. Materials and reagents

Silver nitrate ($AgNO_3$), sodium dodecyl sulfate (SDS), trisodium citrate, chloroauric acid ($HAuCl_4{\cdot}4H_2O$), L-ascorbic acid (AA), sodium borohydride ($NaBH_4$), graphite powder (analytical grade), rhodamine B, ethanol, n-hexanol, cyclohexane, tetraethoxysilane (TEOS), $NH_3{\cdot}H_2O$, Triton X-100, N, N′-methylenebis(acrylamide) (MBA), methacrylic acid, methacrylamide (MAC), poly(acrylamide) (PAA, MW = 3 000 000), aqueous ammonia solution (28 wt%), poly(ethylene glycol) (PEG, MW = 2000), and azobisisobutyronitrile (AIBN) were all purchased from Sinopharm Chemical Reagent (Shanghai, China). Tris(2-carboxyethyl)phosphine (TCEP), polyvinylpyrrolidone (PVP, MW = 55,000), poly(diallyldimethylammonium chloride) solution (PDDA, MW: 200,000–350,000, 20 wt%), 2-trifluoromethacrylic acid (TFMAA), 4-vinylpyridine (4-VPY), Nafion 117 solution (5%), and ethylene glycol dimethacrylate (EGDMA) were provided by Sigma-Aldrich (St. Louis, MO). The RhB labeled DNA probe was obtained from TaKaRa Biotechnology (Dalian, China), and the other DNA sequences with HPLC purification (Table S1) were obtained from Sangon Biotechnology (Shanghai, China). MAA was distilled under reduced pressure to remove the polymerization inhibitor. Clinical human serum samples were collected from a local pathology laboratory and stored at 4 °C. Ultrapure water obtained by Millipore water purification system (≥ 18 MΩ cm, Milli-Q, Millipore) was used throughout the experiments. Phosphate buffer saline (PBS, 0.1 M, pH = 7.4) was prepared with ultrapure water and employed as the supporting electrolyte. The other chemicals and reagents were all of analytical grade and used as received without further purification.

2.2. Instruments

The surface morphologies were observed with scanning electronic microscopy (SEM, HITACHI S-4800, Hitachi, Tokyo, Japan), transmission electron microscopy (TEM, JEOL JEM-2100F), and atomic force microscopy (AFM, Veeco Nanoscope IIIa MultiMode) in tapping mode. The UV–visible (UV–vis) absorption spectra were obtained with UV-1800 spectrophotometer (Shimadzu, Japan). The electrochemical measurements were performed using a CHI 820B electrochemical workstation (CH Instruments, Shanghai, China) with a conventional three-electrode system in 10 mL of glass cell, composed of a modified or bare glassy carbon electrode (GCE, 3 mm in diameter) as working electrode, an Ag/AgCl with saturated KCl solution as reference, and a platinum wire as auxiliary electrode.

2.3. Preparation of SiO_2@Ag/DNA

The preparation procedures of SiO_2@Ag/DNA are illustrated in Scheme 1A. Monodisperse silica nanoparticles were synthesized according to previous literature with some modifications (Fan et al., 2013). The details were provided in the Supporting information. The SiO_2@Ag was prepared according to reported literature (Deng et al., 2007), where 1.0 mL of 0.1 g/mL SiO_2 nanoparticles in aqueous solution was quickly added to 10 mL of freshly prepared $[Ag(NH_3)_2]^+$ solution under magnetic stirring at room temperature. $[Ag(NH_3)_2]^+$ was allowed to absorbed for 1 h onto SiO_2 nanoparticles surface via electrostatic attractions between $[Ag(NH_3)_2]^+$ and negatively charged Si-OH groups. The resulting dispersion was mixed with 50 mL of 5×10^{-4} M PVP ethanol solution placed in a 250 mL three-neck flask under vigorous magnetic stirring at 70 °C for 7 h. The obtained product was then collected by centrifugation (10,000 rpm) and washed at least three times with ultrapure. The resulting SiO_2@Ag was further resuspended

in 1 mL of 5 μM HS-DNA, followed by activation with TCEP (10 mM) and then continuously shaken for 12 h. Finally, SiO_2@Ag/DNA was acquired by centrifugation at room temperature for 10 min. The procedure was performed twice to remove unbound DNA. The particles were finally dispersed in 1.0 mL of 0.1 M PBS for further use.

2.4. Preparation of MIPs film

The composite of AuNPs-GO was prepared according to previous reports with some modification (Han et al., 2012; Zeng et al., 2013), and the details were reported in the Supporting information. A bare GCE was first polished with alumina slurry and washed by ultrapure water under ultrasonication. Next, 5 μL of 1% chitosan solution was dropped on the pretreated GCE and dried in air for 1 h (Scheme 1). Then, 5 μL of 1.0 mg/mL AuNPs-GO solution was cast onto the surface and dried in air. To form MIPs layer, the above modified electrode was immersed into a pre-polymer mixture containing 0.4 mM RhB, 0.5% Nafion, 2.0 mM MAA, 10 mM AIBN and 1.25 mM EGDMA at room temperature. After reaction for 12 h, the resulting electrode was rinsed with 0.1 M HCl containing 10% SDS (w/v) to remove the template. For comparison, nonimprinted polymers (NIPs) coated electrode was prepared with the same procedures as MIPs covered electrodes, with the exception of adding template molecule during the polymerization process.

2.5. Electrochemical detection of T-DNA

The electrochemical detection was performed using differential pulse voltammetry (DPV) in a three-electrode cell configuration. To fabricate the recognizable nanocomposite SiO_2@Ag/dsDNA/RhB, 100 μL of homogeneous DNA solution containing 5 μM RhB-DNA, 0.1 g/mL SiO_2@Ag/DNA and T-DNA at different concentrations in PBS buffer were incubated at 37 °C for 1 h. Next, 5 μL of the hybridization solution was dropped onto the MIPs covered electrode. After incubation in a humidified chamber for 35 min, the electrode was washed with 0.1 M PBS-acetonitrile solution (pH 7.4, 70:30, v/v) for 5 min. Finally, the electrode was dried at room temperature and DPV signals were recorded by CHI 820B in 0.1 M PBS (pH 7.4).

3. Results and discussion

3.1. Characterization of SiO_2@Ag/DNA and MIPs film

The formation of SiO_2@Ag NPs was confirmed by TEM micrographs. Pure SiO_2 NPs with average diameters around 200 nm exhibited uniform size distributions and smooth surfaces (Fig. 1A). After modification with Ag NPs, the surface of SiO_2 NPs was uniformly covered by dark particles (Fig. 1B), indicating the successful preparation of core-shell SiO_2@Ag NPs. UV–vis spectroscopy was employed to confirm the successful synthesis of SiO_2@Ag/DNA. HS-DNA displayed a characteristic peak at 260 nm (Fig. 1C, curve a), attributed to the absorption of purine and thymine bases (Fan et al., 2015; Saito et al., 2012). For SiO_2 nanoparticles, no absorption peaks were observed before the coverage of Ag NPs (Fig. 1C, curve b). On the other hand, the formation of SiO_2@Ag nanoparticles induced an obvious plasmon absorption peak at around 420 nm (Fig. 1C, curve c) attributed to Mie plasmon resonance excitation issued from silver nanoparticles (Deng et al., 2007). The covalent bonding of HS-DNA to SiO_2@Ag NPs through Ag-S induced a characteristic peak of DNA at 260 nm and plasmon absorption peak at 420 nm (Fig. 1C). This demonstrated the successful synthesis of SiO_2@Ag/DNA. The SiO_2@Ag/dsDNA/RhB nanocomposite was constructed by SiO_2@Ag/DNA, T-DNA, and RhB-DNA through homogeneous DNA hybridization was also confirmed by UV–vis shown in Fig. S2.

The FT-IR spectroscopy was employed to investigate the structural changes of MIPs film before and after removal of the template RhB. As shown in Fig. 1D, AuNPs-GO hardly exhibited characteristic absorption peaks. However, the other three materials all presented the characteristic peaks at 2959 cm^{-1} and 2928 cm^{-1}, attributed to stretching vibrations of -CH_3 and -CH_2 in MAA and RhB (Haldorai and Shim, 2014; Su et al., 2015), respectively. The characteristic peak at 1722 cm^{-1} was assigned to the stretching vibration of C=O in carboxyl group and that at 1296 cm^{-1} to stretching vibration in C-N (Liu et al., 2015; Lukose et al., 2015). However, the peak intensity of MIPs before removal of the template appeared stronger. Furthermore, the characteristic vibration peaks of benzene rings in RhB were spotted at 1634 cm^{-1}, 1513 cm^{-1} and 1453 cm^{-1} (Lu et al., 2015), confirming that RhB was successfully imprinted in MIPs. On the other hand, the weakened characteristic peaks displayed by MIPs after removal of the template were indicative of successful synthesis of final MIPs.

To identify the surface topography of NIPs and MIPs, AFM imaging was used in a 2 × 2 μm^2 scanned area. As shown in Fig. S3A, the surface of NIPs film presented a relatively smooth morphology with some bulged block. However, the surface of MIPs film appeared rougher (Fig. S3B). These data further confirmed the successful fabrication of MIPs film.

The molecularly imprinted film was deposited on the electrode by surface imprinting and the electrochemical behaviors were investigated by cyclic voltammogram (CV) and electrochemical impedance spectroscopy (EIS) curves. The electrochemical performances of diverse electrodes could be determined by comparing the CV signals of Fe$(CN)_6^{3-/4-}$ at each electrode. Fig. 1E shows the CV curves of bare GCE, AuNPs-GO modified GCE (AuNPs-GO/GCE), NIPs film modified GCE (NIPs/AuNPs-GO/GCE), and MIPs film modified GCE before and after removal of the template in 5 mM $K_3[Fe(CN)_6]/K_4[Fe(CN)_6]$ solution. Obviously, bare GCE exhibited a couple of reversible redox peaks with peak potential separation (ΔEp) of about 100 mV (Fig. 1E, curve a). After modification with AuNPs-GO, the current intensity increased due to the highly extended surface area and excellent conductivity of AuNPs-GO (Fig. 1E, curve b). Further modification of the electrode by NIPs film decreased the current intensity (Fig. 1E, curve c), indicating the large transfer resistance of polymer film modified GCE. The same was observed for MIPs modified AuNPs-GO/GCE without removal of the template, but with more declined current signal. The latter could be attributed to the large electron transfer resistance of MIPs film containing template when compared to NIPs film. After removal of the template, the current significantly rose thanks to 3D imprinting cavities present in the film, which enhanced the diffusion of Fe$(CN)_6^{3-/4-}$ and accelerated the electron transfer. The EIS results in Fig. 1F are consistent with that of CVs. All of the results demonstrated that the imprinting cavities improved the electrical properties of MIPs film.

3.2. Optimization of imprinting conditions

The molecular imprinting conditions could significantly influence the recognition properties of the obtained MIPs. Hence, the imprinting conditions of MIPs were investigated in terms of monomer type and its concentration, additive and its concentration, and amounts of the template.

The polymerizable monomer directly bonded to the template molecule by noncovalent interaction would be the most important factor affecting the recognition properties of MIPs. Therefore, the appropriate monomer was optimized among MAA, TFMAA, MAC, MBA, and 4-VPY. Using RhB as template, MAA and TFMAA were employed as monomers due to their carboxyl groups, which might bond with two tertiary amino groups of RhB via electrostatic interactions to enhance the interaction between rhodamine B and MIPs (Fig. S4). MAC and MBA were utilized owing to their analogous structures with MAA and amino group binding with oxygen in rhodamine B. 4-VPY was tested because of its positively charged group and pyridine ring, which could interact with RhB via π-π stacking interactions (Cao et al., 2016; Mohamed et al., 2015). As shown in Fig. 2A, MIPs with MAA exhibited the strongest adsorption

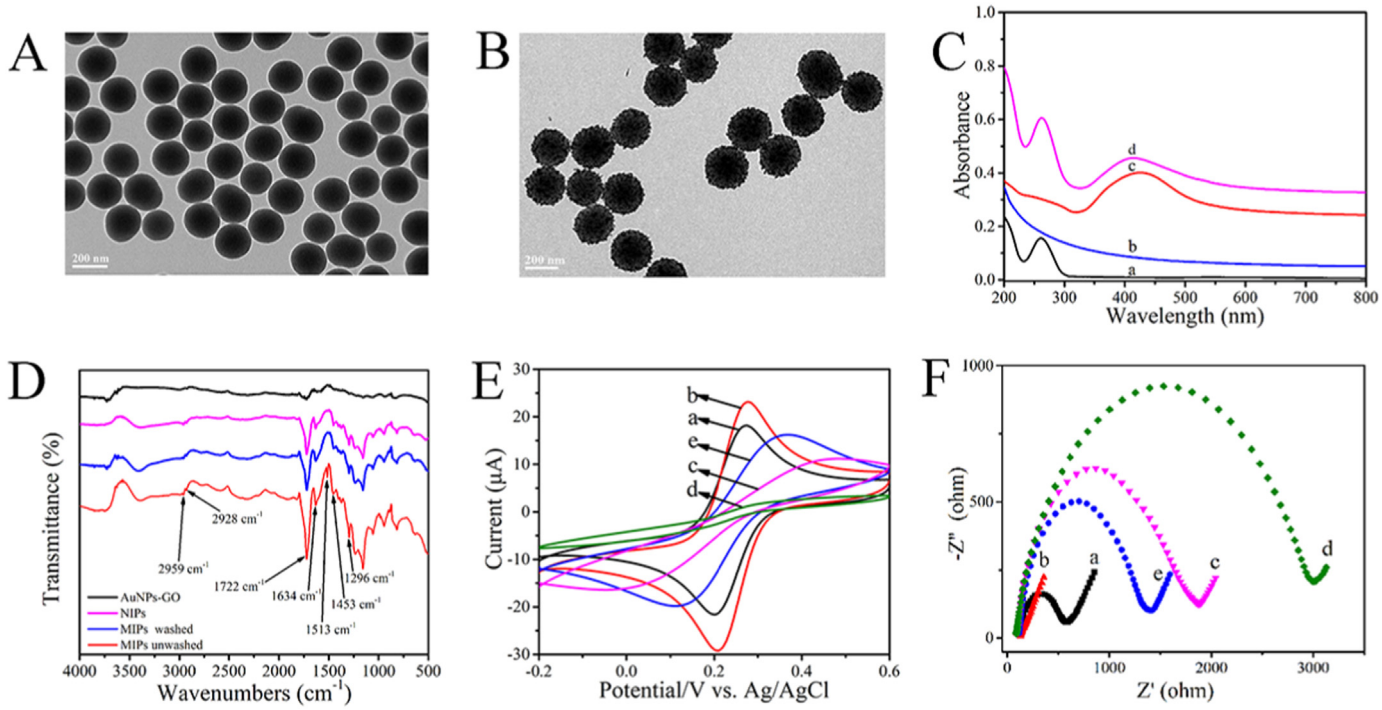

Fig. 1. TEM images of (A) SiO_2 NPs and (B) SiO_2@Ag NPs. (C) UV–vis absorption spectra of HS-DNA (a), SiO_2 NPs (b), SiO_2@Ag NPs (c), and SiO_2@Ag/DNA (d). (D) FT-IR spectra of AuNPs-GO, NIPs, MIPs before and after removal of the template RhB in KBr pressed pellets. CVs (E) and EIS (F) of bare GCE (a), AuNPs-GO/GCE (b), NIPs-AuNPs-GO/GCE (c), and MIPs-AuNPs-GO/GCE before (d) and after (e) removal of the template molecules in 5 mM $K_3[Fe(CN)_6]/K_4[Fe(CN)_6]$ solution containing 0.1 M KCl.

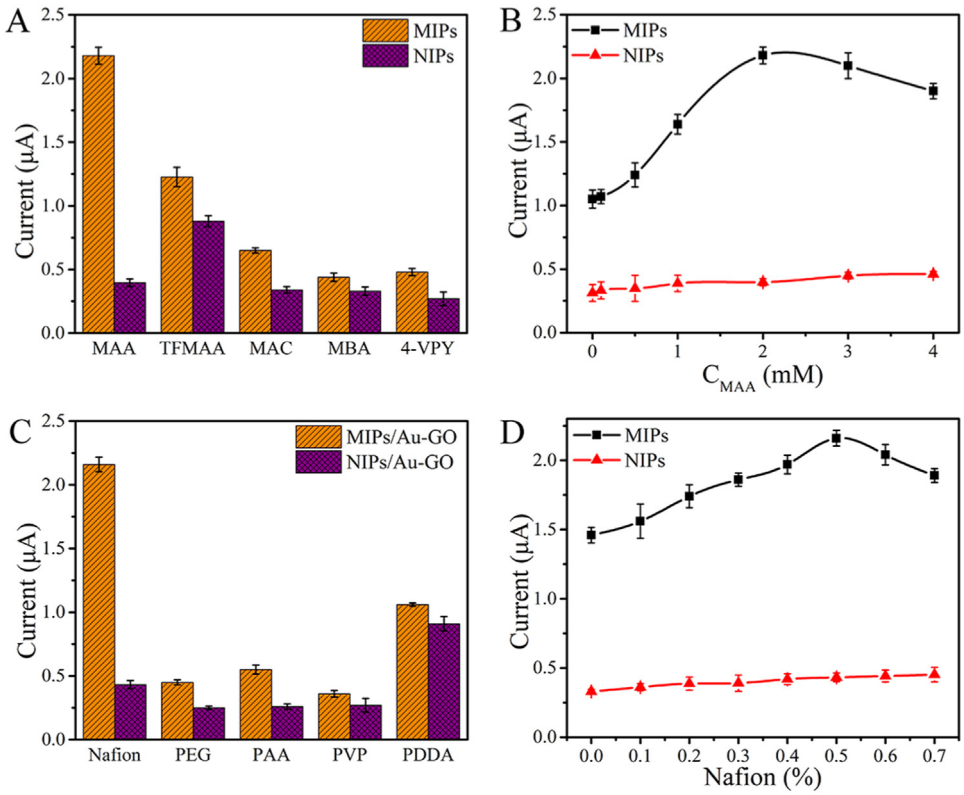

Fig. 2. The DPV peak current responses of MIPs-AuNPs-GO/GCE and NIPs-AuNPs-GO/GCE with 5 μL of SiO_2@Ag/dsDNA/RhB containing 100 nM T-DNA used for optimizing the imprinting conditions: (A) monomers (2 mM), (B) concentrations of MAA, (C) additives (0.5%), and (D) contents of Nafion.

capability on SiO_2@Ag/dsDNA/RhB. This was due to the imprinting cavities in MIPs, matching the three-dimensional shape of RhB and providing enough recognizing sites of carboxyl group. Furthermore, MIPs with MAA revealed the highest imprinting factor (IF) value of 4.9, representing the peak current intensity ratio of SiO_2@Ag/dsDNA/RhB detected on MIPs to that of NIPs under the same conditions. Therefore, MAA was selected as the most appropriate monomer to prepare MIPs.

The concentration of MAA used to prepare MIPs was further optimized. MIPs exhibited improved adsorption performances as MAA concentration increased from 0.1 to 2 mM (Fig. 2B). While, the current response declined beyond 2 mM, since the excess MAA might enhance the density of MIPs and block the electron transfer. Hence, the optimal concentration of MAA was recorded as 2 mM with an IF value of 5.6.

Considering the two positive-charged tertiary amino groups and benzene ring in RhB, polymer additives (including Nafion, PEG, PAA, PVP, and PDDA) with negatively charged groups and π-π stacking interaction were used to improve the absorption of MIPs. It can be seen that MIPs with Nafion had a much higher affinity to SiO_2@Ag/dsDNA/RhB than the others (Fig. 2C). This was ascribed to the sulfonic acid groups generating negatively charged attractions and the fluorine atoms enhancing the electrostatic interactions (Fig. S4). Though PEG and PAA could also provide electron donor and hydrogen to enhance affinity towards RhB, the poor conductivity and dense structure of the polymers would dramatically weaken the current response. PVP could bond to RhB through π-π stacking interactions through the pyrrole ring. However, the poor conductivity of PVP would limit the electrochemical performances. The addition of PDDA to MIPs could generate a stronger current signal but enhanced the response of NIPs, leading to low IF value attributed to the positively charged PDDA interacting with negative-charged phosphate groups in DNA. Consequently, Nafion was selected as the best additive to enhance the adsorption capability of MIPs.

The optimal Nafion content was also investigated in Fig. 2D. Clearly, the current response of MIPs increased as Nafion content rose from 0% to 0.5%, followed by a gradual reduction. This indicated that MIPs with 0.5% Nafion could display the most excellent recognition capability towards RhB with an IF value of 5.2.

The amount of template could directly affect the number of imprinting cavities on MIPs, determining the quantity of SiO_2@Ag/dsDNA/RhB binding to MIP film. Fig. S5 illustrated that the peak current of MIPs continuously increased at RhB concentrations ranging from 0 to 0.4 mM and then kept constant. This suggested that the growing template could enhance the adsorption of SiO_2@Ag/dsDNA/RhB on MIPs. However, the adsorption reached a kinetic balance at RhB concentration exceeding 0.4 mM. Therefore, 0.4 mM RhB was selected as the optimal concentration to prepare MIPs.

3.3. Optimization of detection conditions

To achieve the optimal detection sensitivity of T-DNA, the concentration of RhB-DNA, DNA hybridization time, pH of incubating solution, incubation time for recognizing SiO_2@Ag/dsDNA/RhB, and washing time for removal of the nonspecifically adsorbed nanocomposites were systematically explored. As the RhB-DNA concentration rose from 0.1 to 5 μM, the peak current increased due to more bonding between SiO_2@Ag/dsDNA/RhB and MIPs (Fig. 3A). However, excess RhB-DNA might prevent electron transfer of the MIPs film, leading to the decreased current responses beyond 5 μM RhB-DNA.

Fig. 3B presents the effect of DNA hybridization time on the detection sensitivity from 10 to 120 min. The continuously increased current responses were visible within the first 60 min and then remained nearly constant as hybridization time further prolonged. Hence, 60 min was determined as the optimal hybridization time and used for further studies.

The effect of pH values, influencing the recognition performance of MIPs, is illustrated in Fig. 3C. The peak current showed a positive response towards pH value ranging from 4 to 6, reflecting the improved recognition of MIPs. However, the current intensity dramatically dropped in the pH range of 6–9, indicating that pH beyond 6 prevented binding of MIPs. Therefore, MIPs exhibited excellent recognition performances in weak acid conditions (pH = 6).

The peak current responses of SiO_2@Ag/dsDNA/RhB with MIPs at different incubation time are shown in Fig. 3D. Prolonged incubation time clearly enhanced the current signals from 5 to 35 min. Nevertheless, stable DPV responses after 35 min were obtained. Under the optimized conditions, the IF value achieved 4.9. Therefore, 35 min was selected as the optimal incubation time and applied to MIPs binding with SiO_2@Ag/dsDNA/RhB.

Fig. S6 depicts the effect of washing time on peak current responses obtained from MIPs and NIPs films. The responses of both films decreased with increasing washing time from 1 to 11 min, but IF achieved the highest value at 5 min. Hence, 5 min was selected as the optimal washing time and used for further studies.

3.4. Analytical performances of biosensor

The electrochemical response of SiO_2@Ag/dsDNA/RhB on MIPs/AuNPs-GO/GCE was further investigated by comparing with AuNPs-GO/GCE, Nafion/AuNPs-GO/GCE, MAA/AuNPs-GO/GCE, NIPs/AuNPs-GO/GCE, and MIPs/AuNPs-GO/GCE. As shown in Fig. 4A, AuNPs-GO/GCE (green line) exhibited a weak electrochemical signal, indicating low ability to recognize SiO_2@Ag/dsDNA/RhB. After modification with NIPs, a relatively stronger current response of NIPs-AuNPs-GO/GCE (magenta line) was recorded due to the physical adsorption by the polymer. The Nafion/AuNPs-GO/GCE (red line) and MAA/AuNPs-GO/GCE (blue line) were prepared by the same procedures as MIPs/AuNPs-GO/GCE, but without the addition of MAA and Nafion. Both electrodes exhibited greatly increased current responses when compared to NIP-AuNPs-GO/GCE, showing that both could present good affinities towards SiO_2@Ag/dsDNA/RhB. Hence, modification of AuNPs-GO/GCE by MIPs containing Nafion and MAA resulted in enhanced current signals, demonstrating the special recognition of MIPs/AuNPs-GO/GCE toward SiO_2@Ag/dsDNA/RhB.

The current responses of MIPs and NIPs at different concentrations of T-DNA are shown in Fig. 4B under the optimized conditions. The adsorption isotherms of the MIPs and NIPs substrates were established by plotting the peak current intensities against the logarithm of T-DNA concentrations. For RhB-imprinted MIPs, the peak current intensity apparently increased with the logarithm of T-DNA concentration from 10 fM to 1 μM. By comparison, the current response of NIPs under identical conditions exhibited a slightly increased current response as T-DNA concentration rose. The IF of MIPs was estimated from the two response curves as 8.5 (based on maximum binding amounts of MIPs and NIPs). This indicated the significant binding affinity of the MIPs towards T-DNA.

Fig. 4C shows the DPV responses of T-DNA at different concentrations recorded on MIPs/AuNPs-GO/GCE through the specific capture of SiO_2@Ag/dsDNA/RhB by MIPs at the optimal conditions. The peak current clearly increased as T-DNA concentration rose. A proportional linear correlation between the peak current and logarithm of T-DNA concentrations was further deduced from 10 fM to 100 nM (Fig. 4D), which could be described by the equation: I (μA) = 0.263 $\lg C_{\text{T-DNA}}$ + 3.98 (R^2 = 0.996). The detection limit was calculated as 2.53 fM (S/N = 3). The analytical performances of MIPs/AuNPs-GO/GCE for T-DNA were compared with those of other reported electrochemical DNA approaches and the results are listed in Table S2. The wider linear range and lower detection limit demonstrated the excellent prospects of the proposed strategy based on MIPs to capture targets from homogeneous solutions.

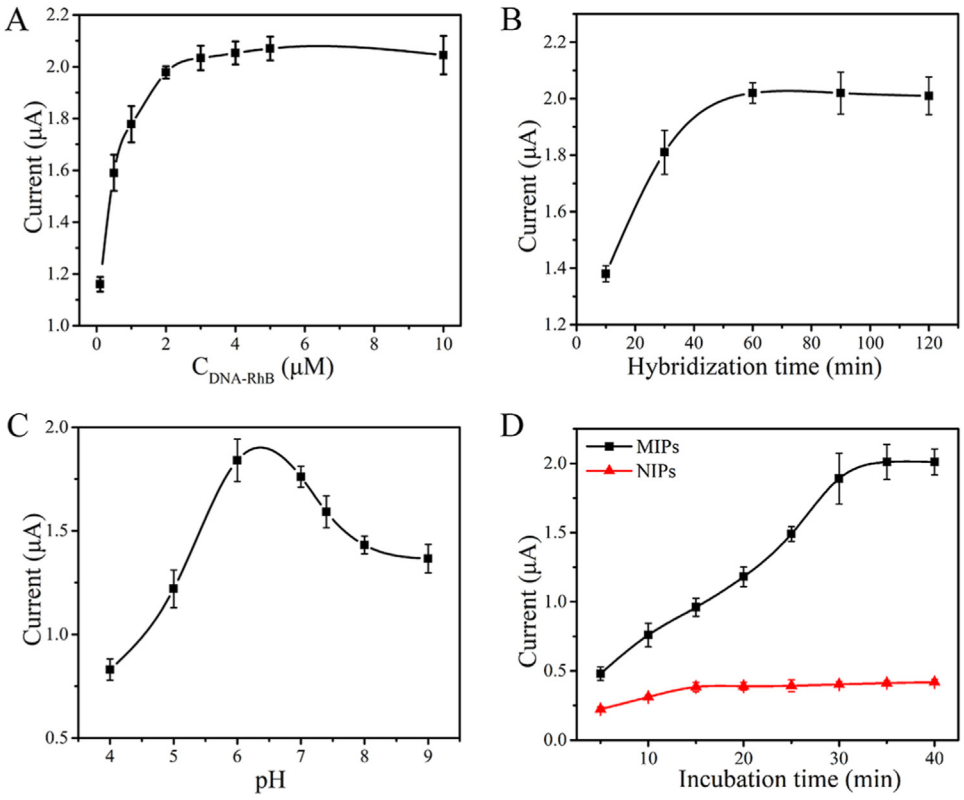

Fig. 3. (A) Current response of SiO_2@Ag/dsDNA/RhB deposited on MIPs film with different concentrations of RhB-DNA. (B) Dependence of peak current intensity on hybridization time. (C) Effects of pH value on recognition of SiO_2@Ag/dsDNA/RhB with MIPs. (D) Optimization of incubation time with MIPs and NIPs films. The concentration of T-DNA is 100 nM in the homogeneous hybridization.

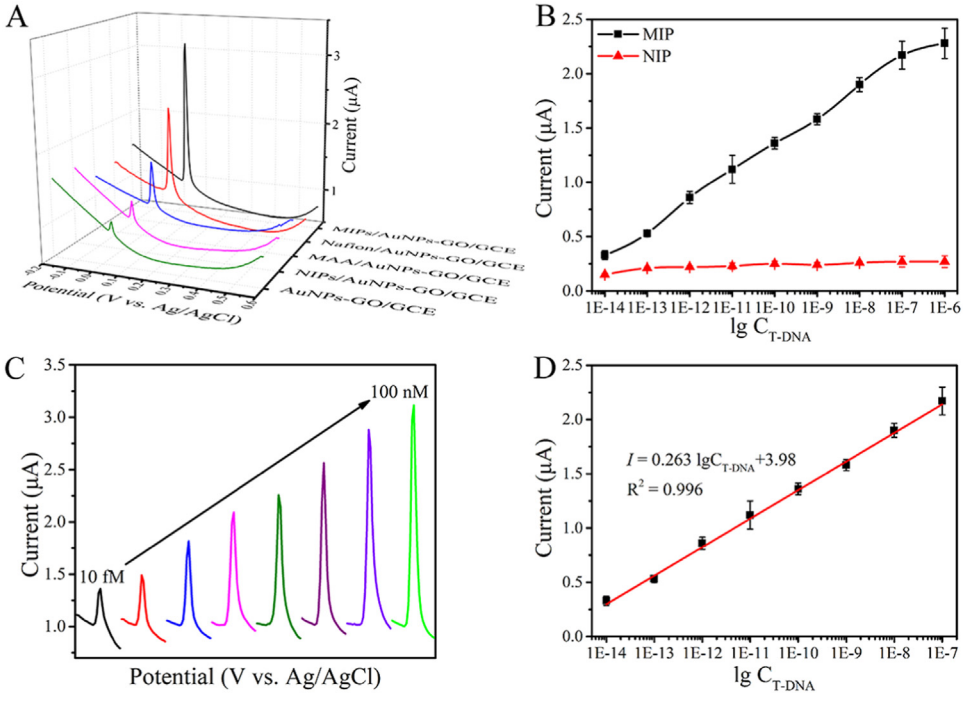

Fig. 4. (A) DPV responses of AuNPs-GO/GCE, NIPs/AuNPs-GO/GCE, MAA/AuNPs-GO/GCE, Nafion/AuNPs-GO/GCE, and (d) MIPs/AuNPs-GO/GCE in 0.1 mM PBS (pH 7.4) after incubation with SiO_2@Ag/dsDNA/RhB for 35 min. The concentration of T-DNA in the homogeneous hybridization is 100 nM. (B) Peak current intensity detected on RhB-imprinted substrate MIPs and NIPs at different T-DNA concentrations. (C) DPV curves of RhB-imprinted substrate MIPs. (D) calibration curve used for detection of T-DNA from 10 fM to 100 nM. (For interpretation of the references to color in this figure legend, the reader is referred to the web version of this article.)

3.5. Selectivity, reproducibility and stability of MIPs biosensor

To investigate the selectivity of the proposed E-DNA biosensor, DPV signals of single-base (M_1), three-base (M_3) mismatched sequences, and random DNA sequence (Random) were all collected and compared with that of target sequence. All mismatched and random sequences displayed distinguishable peak currents from target DNA (Fig. S7). This excellent selectivity might be attributed to strict principle of complementary base pairing and specific recognition of MIPs, which enlarged the distinctive current signals.

The reproducibility of MIPs biosensor was tested using twelve modified electrodes prepared under the same conditions. A relative standard deviation (RSD) of 7.4% was calculated using the DPV responses of Fig. S8A, indicating the good reproducibility of the proposed MIPs biosensor. The stability was also evaluated by detecting the current responses of the same electrodes stored at 4 °C every 10 days (Fig. S8B). After one month, the signal intensity retained about 93% of the initial values, revealing the excellent stability of the MIPs biosensor.

Table 1
Analysis of T-DNA in clinical human serum samples (n = 3).

Sample	Added (nM)	Found (nM)	Recovery (%)	RSD (%)
1	0	0.01	–	–
2	0.1	0.098	98.0	1.1
3	0.5	0.49	98.0	1.6
4	1.0	0.97	97.0	3.1
5	5.0	5.16	103.2	7.2
6	10.0	10.64	106.4	4.3

3.6. Analysis of human serum samples

To determine the practical performances of the proposed method, the recovery of T-DNA at concentrations of 0, 0.1, 0.5, 1.0, 5.0, and 10.0 nM were analyzed in 10 folds diluted human serum samples (Table 1). The recovery values were estimated between 97% and 106.4% with acceptable RSD values. This indicated the potential application of the proposed MIPs-based biosensor in clinical applications.

4. Conclusions

In summary, a novel homogeneous E-DNA biosensing strategy has been successfully developed using MIPs to capture homogenously the hybridized DNA nanocomposites–SiO_2@Ag/dsDNA/RhB, where SiO_2@Ag was employed as both the electrochemical indicator and signal amplifier. MIPs film was prepared on the AuNPs-GO modified electrode with RhB as the template and Nafion as additive. The selective recognition of MIPs for SiO_2@Ag/dsDNA/RhB was contributed by the shape matching of imprinting cavities and electrostatic interactions between Nafion and RhB. Under the optimized conditions, the fabricated MIPs-based electrochemical DNA biosensing strategy yielded high sensitivity down to 2.53 fM in homogeneous solution, attributing to the amplification of SiO_2@Ag. Furthermore, the application of the proposed method was evaluated with the determination of BRCA-1 in human serum samples, exhibiting the satisfactory results. The proposed MIPs-based biosensing method could potentially be extended for the detection of other biomolecules in biochemical research and early diagnosis of diseases.

Acknowledgements

This work was financially supported by the National Natural Science Foundation of China (No. 21575042 and No. 21405049).

Appendix A. Supporting information

Supplementary data associated with this article can be found in the online version at http://dx.doi.org/10.1016/j.bios.2018.04.038.

References

Becker, B., Cooper, M.A., 2011. J. Mol. Recognit. 24 (5), 754–787.
Cao, Y., Sui, D., Zhou, W., Lu, C., 2016. Sens. Actuators B 225, 600–606.
Cui, H.F., Cheng, L., Zhang, J., Liu, R., Zhang, C., Fan, H., 2014. Biosens. Bioelectron. 56, 124–128.
Deng, Z., Chen, M., Wu, L., 2007. J. Phys. Chem. C 111 (31), 11692–11698.
Diculescu, V.C., Chiorcea-Paquim, A.M., Oliveira-Brett, A.M., 2016. TrAC Trends Anal. Chem. 79, 23–36.
Drummond, T.G., Hill, M.G., Barton, J.K., 2003. Nat. Biotechnol. 21 (10), 1192–1199.
Du, Y., Dong, S., 2017. Anal. Chem. 89 (1), 189–215.
Fan, G.C., Zhu, H., Shen, Q., Han, L., Zhao, M., Zhang, J.R., Zhu, J.J., 2015. Chem. Commun. 51 (32), 7023–7026.
Fan, H.J., Wang, X.L., Jiao, F., Zhang, F., Wang, Q.J., He, P.G., Fang, Y.Z., 2013. Anal. Chem. 85, 6511–6517.
Farjami, E., Clima, L., Gothelf, K., Ferapontova, E.E., 2011. Anal. Chem. 83 (5), 1594–1602.
Haldorai, Y., Shim, J.J., 2014. Appl. Surf. Sci. 292 (4), 447–453.
Han, J., Zhuo, Y., Chai, Y.Q., Yuan, Y.L., Yuan, R., 2012. Biosens. Bioelectron. 31 (1), 399–405.
Hong, N., Cheng, L., Wei, B., Chen, C., He, L.L., Kong, D., Ceng, J., Cui, H.F., Fan, H., 2017. Biosens. Bioelectron. 91, 110–114.
Ling, P., Lei, J., Zhang, L., Ju, H., 2015. Anal. Chem. 87 (7), 3957–3963.
Liu, L., Zhong, T., Xu, Q., Chen, Y., 2015. Anal. Chem. 87 (21), 10910–10919.
Lu, L., Yue, X., Lin, F., Huang, F., Zhang, B., Lin, 2015. J. Mater. Chem. A 3 (20), 10959–10968.
Lukose, J., Yohannan Panicker, C., Nayak, P.S., Narayana, B., Sarojini, B.K., Van Alsenoy, C., Al-Saadi, A.A., 2015. Spectrochim. Acta Part A 135, 608–616.
Mahshid, S.S., Camire, S., Ricci, F., Vallee-Belisle, A., 2015. J. Am. Chem. Soc. 137 (50), 15596–15599.
Mohamed, M.G., Lu, F.H., Hong, J.L., Kuo, S.W., 2015. Polym. Chem. 6 (35), 6340–6350.
Nagai, S., Miyamoto, S., Ino, K., Tajimi, S., Nishi, H., Tomono, J., 2016. Harmful Algae 51, 97–106.
Palecek, E., Bartosik, M., 2012. Chem. Rev. 112 (6), 3427–3481.
Saito, S.T., Silva, G., Pungartnik, C., Brendel, M., 2012. J. Photochem. Photobiol. B 111, 59–63.
Schirhagl, R., 2014. Anal. Chem. 86 (1), 250–261.
Su, X., Li, X., Li, J., Liu, M., Lei, F., Tan, X., Li, P., Luo, W., 2015. Food Chem. 171, 292–297.
Tiwari, A., Deshpande, S.R., Kobayashi, H., Turner, A.P., 2012. Biosens. Bioelectron. 35 (1), 224–229.
Tretyakova, N., Villalta, P.W., Kotapati, S., 2013. Chem. Rev. 113 (4), 2395–2436.
Wackerlig, J., Schirhagl, R., 2016. Anal. Chem. 88 (1), 250–261.
Wang, Q., Wang, W., Lei, J., Xu, N., Gao, F., Ju, H., 2013. Anal. Chem. 85 (24), 12182–12188.
Wang, W., Ge, L., Sun, X., Hou, T., Li, F., 2015. ACS Appl. Mater. Interfaces 7 (51), 28566–28575.
Xiao, Y., Lou, X., Uzawa, T., Plakos, K.J., Plaxco, K.W., Soh, H.T., 2009. J. Am. Chem. Soc. 131 (42), 15311.
Yoshikawa, M., Tharpa, K., Dima, S.O., 2016. Chem. Rev. 116 (19), 11500–11528.
Zeng, Y.B., Zhou, Y., Kong, L., Zhou, T.S., Shi, G.Y., 2013. Biosens. Bioelectron. 45, 25–33.
Zhang, C.-Y., Yeh, H.-C., Kuroki, M.T., Wang, T.-H., 2005. Nat. Mater. 4 (11), 826–831.
Zhang, F.T., Cai, L.Y., Zhou, Y.L., Zhang, X.X., 2016. TrAC Trends Anal. Chem. 85, 17–32.
Zhang, H., Li, F., Dever, B., Li, X.F., Le, X.C., 2013. Chem. Rev. 113 (4), 2812–2841.
Zhao, Y., Chen, F., Li, Q., Wang, L., Fan, C., 2015. Chem. Rev. 115 (22), 12491–12545.